PCCP

Accepted Manuscript

ROYAL SOCIETY OF CHEMISTRY

www.rsc.org/pccp

A Comprehensive Study of Sulfonated Carbon Materials as Conductive Composites for Polymer Solar Cells

Ting Ji[1], Licheng Tan[1,2], Xiaotian Hu[1], Yanfeng Dai[1], Yiwang Chen[*1,2]

[1]College of Chemistry/Institute of Polymers, Nanchang University, 999 Xuefu Avenue, Nanchang 330031, China; [2]Jiangxi Provincial Key Laboratory of New Energy Chemistry, Nanchang University, 999 Xuefu Avenue, Nanchang 330031, China

Abstract

Sulfonated carbon nanotubes (S-CNTs) and sulfonated graphenes (S-Gra) with superior dispersibility have been successfully prepared to modify poly(3,4-ethylenedioxythiophene):poly(styrenesulfonate) (PEDOT:PSS) for application in polymer solar cells (PSCs). The synergetic effect between S-CNTs/ S-Gra and PEDOT:PSS could remove excess insulating PSS chains leading to obvious phase separation between the PEDOT and PSS chains, which allowing the formation of more conductive PEDOT channels. The PEDOT:PSS (Clevios PH 4083):S-CNTs with well-matched work function, favorable morphology, optimized hydrophobicity and superior hole mobility is demonstrated to be an excellent hole transport layer (HTL) for PSCs. But the PEDOT:PSS (Clevios PH 4083) modified by sulfonated graphenes with stacked and wrinkled lamellas as HTL rendering the rough morphology results in negative impact on the morphology of active layer, consequently poor device performance. Excitingly, PEDOT:PSS (Clevios PH 1000) modified with S-Gra shows high conductivity, because of sulfonated graphene lamellas contributing to the connection among insular and conductive PEDOT islands and improving charge conduction. The PH1000:S-Gra with multiple layers presents excellent electrical conductive properties and high transmittance (sheet resistance of ~

[*] Corresponding author. Tel.: +86 791 83969562; fax: +86 791 83969561. *E-mail address*: ywchen@ncu.edu.cn (Y. Chen).

45 Ω sq^{-1} and transmittance of ~ 85.5% at 550 nm), which possessing great potential for usage as a transparent conductive and flexible electrode in organic electronics.

Keywords: carbon nanotubes; graphenes; polymer solar cells; hole transport layer; conductive composites

1. Introduction

Organic photovoltaics (OPVs) are receiving considerable attention due to their potential for environmentally-friendly, low-cost energy harvesting, solution processible and printable, portable and renewable energy sources[1,2]. In the last few years, high performance polymer solar cells (PSCs) based on bulk heterojunction (BHJ) structures have been reported with efficiencies up to 10%, which provides impetus for the next generation organic photovoltaic devices, hence leading to 4th generation (4G) hybrid solar cells[3,4] and their successful commercialization[5-7]. The research field of PSCs has diversified into at least three overlapping fractions: high power conversion efficiency, stability and compatibility to printing or roll-to-roll technique, which are the most crucial considerations for obtaining commercialization of PSCs.

Polymer solar cells are consisted of photoactive layer, interfacial buffer layers, and electrodes. Photoinduced charges generation and dissociation are mainly dominated by the optical and electrical properties of the active layer, so substantial efforts are underway in the scientific community to improve the optical absorption and charge generation in the photoactive layer[8,9]. Moreover, the fabrication of efficient interfacial transporting layers (ITLs) used between the active layer and the electrodes requires equal scientific endeavor[10,11], because the charges transport-extraction process depends critically on ITLs. The adequate ITLs can prevent recombination of electrons and holes by providing selective and fast carrier transportation efficiency[12], thus, they have a direct effect on the overall performance of OPVs. Several key factors such as transparency, conductivity, passivation property, film morphology, stability, and

solution-processability have been considered for the usage of these promising interfacial layers[13].

The conducting polymer poly(3,4-ethylenedioxythiophene):poly(styrenesulfonate) (PEDOT:PSS) with a high work function (5.2 eV) has been most commonly used as a hole transport layer (HTL) in PSCs to improve holes collection at the anode. However, PEDOT:PSS has several problems including high acidity, hygroscopic properties and inhomogeneous electrical properties, resulting in poor long-term stability[5]. Promising replacements and currently heavily investigated substitutes for PEDOT:PSS come from the class of transition metal oxides (MO), including MoO_3[11],V_2O_5[14,15], NiO[16], SbO_3[17] and WO_3[18-21]. The normal methods of depositing these metal oxides films are the cost-intensive vacuum techniques that are incompatible with low-cost solution-processable and roll-to-roll processed PSCs. Over the past few years, much effort has been expended in searching new solution-processed HTL with potential improvement on the holes transport and collection, particularly at the anode interface. However, the performance is still limited.

The amazing processability of PEDOT:PSS make it still possess great growth prospects. So, another potential method for solution-processed anode interfacial layer is to modify PEDOT:PSS by overcoming the weaknesses of PEDOT:PSS such as low electrical conductivity and poor adherence with the substrate or active layer, which frequently resulting in devices with low efficiency. Several techniques have been employed to improve the PEDOT:PSS features, for instance, post-deposition treatment or usage of additives in the precursor solution as glycol and glycerol. Natasha *et al.*[22] reported that the sheet resistance of the modified PEDOT:PSS with

hexafluroacetone (HFA) decreased and its positive charge carrier injection/collection improved. Besides, pre- and/or post-treatment with various materials including organic polar solvents, surfactants, salts, and acids have also been found to enhance the conductivity (σ_{dc}) of PEDOT:PSS by two to three orders of magnitude. And PEDOT:PSS treated with 100% sulfuric acid showed a high conductivity (σ_{dc} = 4380 $S \cdot cm^{-1}$)[23], which was comparable to that of indium tin oxide (ITO) (5000 $S \cdot cm^{-1}$). In addition, the effects of using additives on the surface tension of PEDOT:PSS solution and the electrical properties of the resulting films have also been studied, which arising from the morphological changes.

Recently, carbon materials including carbon nanotubes (CNTs) and graphenes have gained great attention due to their excellent electrical, optical, chemical, and mechanical properties. CNTs and graphenes offer good durability and flexibility, ease of processing, low reflectance, natural color, and stable transparency along the whole visible light spectrum. The transistor devices based on the random single-walled carbon nanotube (SWCNT) network films show much higher mobility (ca.~100 cm^2 V^{-1} s^{-1})[24] than that based on polymer. The mobility of transistors with aligned SWCNTs arrays even reaches 2000 cm^2 V^{-1} s^{-1}. To a certain extent, compositing CNTs and PEDOT:PSS is able to complement both of their disadvantages. On one hand, the addition of conductive CNTs can remove excess insulating PSS and build bridges or networks for connecting the conductive PEDOT grains. On the other hand, the conductive nature of PEDOT:PSS among CNTs networks can decrease the contact resistance of CNTs induced by tube-tube junctions[24]. Nevertheless, CNTs has an intrinsic problem of insolubility in most solvents which many approaches have been carried out to solve in decades. The oxidation of CNTs and grafting of polymer onto

CNTs are the most widely utilized methods to improve the solubility of CNTs in solvents[25,26]. Yun et al.[26] has explored the effect of different CNTs oxidation approaches on the properties of PEDOT:PSS/CNTs composite film, such as surface roughness, work function, surface energy, optical transparency and conductivity. Studies on the application of CNTs, PEDOT:PSS and/or CNT/PEDOT:PSS composites as electrodes in organic light emitting diode (OLED) and catalytic counter electrode (CCE) in dye sensitized solar cells (DSSC) have been reported.

In this work, the carbon materials were functionalized by concentrated sulfuric acid, resulting in sulfonated carbon nanotubes (S-CNTs) and sulfonated graphenes (S-Gra) used to modify PEDOT:PSS with different concentration. The synergetic effect between sulfonated carbon materials and PEDOT:PSS could remove excess insulating PSS chains leading to obvious phase separation between the PEDOT and PSS chains, which allowing the formation of more conductive PEDOT channels, and consequently enhance the conductivity of the composites. The polymer solar cells performances based on PEDOT:PSS (Clevios PH 4083) and sulfonated carbon materials as hole transport layers demonstrated that PEDOT:PSS:S-CNTs provided a proper interfaces due to favorable morphology and improved conductivity with comparison to PEDOT:PSS:S-Gra. Besides, PEDOT:PSS (Clevios PH 1000) modified by sulfonated graphenes with high conductivity and transparency were also demonstrated to own great potential for applications in organic electronics as transparent conductive and flexible electrodes.

2. Experimental Section

2.1. Materials and preparation

The pristine carbon nanotubes (P-CNTs) and graphenes (purchased from Sigma Aldrich) were sulfonated with concentrated sulfuric acid[27,28] (See Supporting Information). Then P-CNTs, S-CNTs and S-Gra were dispersed in dimethyl sulfoxide (DMSO, 1 mg/mL) through 1 h ultrasonic treatment. For the post-treatments, the P-CNTs, S-CNTs and S-Gra dispersion were added into PEDOT:PSS (Clevios PH 4083, purchased from Heraeus Ltd.) aqueous solutions, the weight ratios of various carbon materials in the PEDOT:PSS is 0.1%, 0.2%, 0.4%, respectively. To make a comparison, DMSO solvent was also immersed into PEDOT:PSS with the same volume ratios as the carbon materials dispersion. These samples were named as PEDOT:PSS:P-CNTs, PEDOT:PSS:S-CNTs, PEDOT:PSS:S-Gra, PEDOT:PSS:DMSO, respectively. Besides, P-CNTs, S-CNTs and S-Gra with 1% weight ratio were added into PEDOT:PSS (Clevios PH 1000, purchased from Heraeus Ltd.) aqueous solution, respectively, then were filtered using a hydrophilic syringe filter (0.45 μm) to remove large-size particles. The samples were defined as PH1000:P-CNTs, PH1000:S-CNTs and PH1000:S-Gra, respectively.

2.2. Fabrication of PSCs

The polymer solar cells were fabricated on glass substrates. ITO-coated glass substrates were first cleaned by ultrasonic agitation in acetone, detergent, deionized water, and isopropanol sequentially, followed by drying with nitrogen flow and UV treatment for 20 min. After cleaning, PEDOT:PSS:P-CNTs, PEDOT:PSS:S-CNTs, PEDOT:PSS:S-Gra aqueous solutions with various weight ratios (0.1%, 0.2%, 0.4%) were spin-coated on ITO-coated glass substrates at a speed of 4000 rpm for 60 s, respectively. The thickness of modified PEDOT:PSS film has been measured by surface profilometer to be about 30 nm. The composite films were annealed at 140 ℃

for 15 min in ambient air. The regioregular poly(3-hexylthiophene-2,5-diyl) (P3HT, 20 mg, Mw = 48300 g/mol, head-to-tail, regioregularity > 90%, Rieke Metals, Inc.) and [6,6]-phenyl-C61-butyric acid methyl ester (PCBM, 20 mg, 99.5% purity, Nano-C) were dissolved in 1,2-dichlorobenzene solution (P3HT:PCBM, 1:1 w/w). Then the P3HT:PCBM blend was spin-coated on top of the composite layers, and natural cooled at glove box for 2 h, and then thermally annealed at 150 °C for 10 min. Finally, 7 nm LiF and 100 nm Al were deposited by thermal evaporation through a shadow mask to form an active area of 4 mm. The PH1000:P-CNTs, PH1000:S-CNTs and PH1000:S-Gra aqueous solutions were spin-coated on glass substrates at a speed of 2000 rpm for 60 s, then were annealed at 140 °C for 20 min in ambient air.

2.3. Characterization of PSCs

The light source was calibrated by using silicon reference cells with an AM 1.5 global solar simulator (intensity of 100 mW/cm^2). The current-voltage (*J-V*) characteristics were recorded using Keithley 2400 source meter (Abet Solar Simulator Sun2000). All the measurements were performed under ambient atmosphere at room temperature.

3. Results and Discussion

Due to the pristine carbon materials existing the shortcomings of insolubility and low dispersibility in solvents, severe aggregation and inherently poor compatibility with conductive polymer, pristine carbon nanotubes (P-CNTs) and graphenes were functionalized[28,27] by concentrated sulfuric acid, obtaining sulfonated carbon nanotubes (S-CNTs) and sulfonated graphenes (S-Gra). The resultant S-CNTs and S-Gra were investigated by X-ray photoelectron spectroscopy (XPS), Raman, Fourier transform infrared spectroscopy (FT-IR), scan electron microscopy (SEM), transmission electron microscopy (TEM), energy dispersive spectrometer (EDS) and

X-ray diffraction (XRD), as shown in **Figure S1**. FT-IR and EDS analysis illustrate sulfonic acid (-SO_3H) groups have been covalently bonded to carbon materials. The contents of elemental sulfur (S) in S-CNTs and S-Gra are estimated to be 2.35 atom% and 1.08 atom% by XPS, respectively. The Raman spectra of the carbon materials shows a slightly changes in the I_D/I_G ratio before and after sulfonation treatment[29]. Likewise, the corresponding XRD patterns and TEM microscopic characterizations also prove that the sulfonated carbon materials with dramatic morphological change have been obtained by functionalization. Furthermore, the sulfonated carbon materials processed better dispersibility, as shown by SEM images in **Figure S2.**

The incorporation of sulfonated carbon materials may overcome the weaknesses of PEDOT:PSS such as low electrical conductivity, which may be beneficial for the composite films as solution-processed hole transport layer (HTL) applied in polymer solar cells. The device structures with different modified PEDOT:PSS films as HTL are shown in **Figure 1**. The PEDOT:PSS solution treated with S-CNTs, P-CNTs and S-Gra at different ratios were spin-coated on top of ITO at 4000 rpm/min. The *J-V* curves acquired AM 1.5 illumination for ITO/HTL/P3HT:PCBM/LiF/Al devices are shown in **Figure 1**, and the corresponding photovoltaic characteristics are listed in **Table 1**. The control P3HT:PCBM bulk heterojunction device (with pristine PEDOT:PSS) showed a short-circuit current density (J_{sc}) of 8.95 mA/cm^2, an open-circuit voltage (V_{oc}) of 0.58 V, and a fill factor (FF) of 0.60, resulting in a power conversion efficiency (PCE) of 3.15%. In order to exclude the possibility of the effect of the solvent dimethylsulfoxide (DMSO) on device performance, a reference device was also fabricated by spin-coating PEDOT:PSS treated with pure DMSO solvent on the top of ITO. The different volume DMSO-treated devices show almost the same

performance as the control one. From the results of the photovoltaic characteristics of the modified PEDOT:PSS by S-CNTs, P-CNTs, S-Gra with different weight ratios, respectively, the superior photovoltaic performance is observed in the device based on PEDOT:PSS treated by sulfonated carbon materials (S-CNTs and S-Gra) at 0.2% weight ratio. When spin-coated from the PEDOT:PSS solution added with sulfonated carbon materials with high weight ratio, the film-forming property of the solution became weaker, resulting an rough and discontinuous interface. In addition, the device shows the best photovoltaic performance with PCE values up to 3.91%, J_{sc} of 10.49 mA/cm^2, V_{oc} of 0.58 V, and FF of 64.1%. For the devices based on modified PEDOT:PSS:S-CNTs (0.2%), the average device efficiency is more than 3.9% (as shown in Supporting Information **Figure S3**), which shows the good reproducibility of this method. Nevertheless, inserting PEDOT:PSS:P-CNTs and PEDOT:PSS:S-Gra as HTL do not remarkably improve the photovoltaic performance. The device based on PEDOT:PSS:P-CNTs (0.2%) exhibits poor device performance with a V_{oc} of 0.59 V, J_{sc} of 7.15 mA/cm^2, FF of 62.4%, PCE of 2.63%, and PEDOT:PSS/S-Gra (0.2%) with a V_{oc} of 0.57V, J_{sc} of 7.95 mA/cm^2, FF of 62.9%, PCE of 2.90%. The above results indicates that the device with PEDOT:PSS:S-CNTs (0.2%) as HTL presents superior photovoltaic performance due to the higher current density and FF than those of PEDOT:PSS:P-CNTs (0.2%) and PEDOT:PSS:S-Gra (0.2%). From the corresponding dark *J-V* characteristics shown in **Figure 1**, the device with PEDOT:PSS:P-CNTs (0.2%) and PEDOT:PSS:S-Gra (0.2%) exhibits higher leakage current with respect to that of PEDOT:PSS:S-CNTs (0.2%), the data of which is consistent with the photovoltaic performance (lower current density and FF), and indicates that the PEDOT:PSS modified with P-CNTs and S-Gra may not form uniform and useful interfacial layer morphologies due to the agglomerative pristine

CNTs, and stacked and crumpled lamellar graphenes in the PEDOT:PSS. **Figure 1** also displays log *J vs*. log*V* plotted for Mott-Gurney SCLC fitting of hole-only devices (ITO/modified PEDOT:PSS/P3HT:PCBM/MoO_3/Ag), measured at ambient temperature. Compared to the pristine PEDOT:PSS (only 7.86×10^{-4} cm^2 V^{-1} s^{-1}), the hole mobility of PEDOT:PSS:S-CNTs is remarkably enhanced to 3.58×10^{-3} cm^2 V^{-1} s^{-1}, with about a five-fold increase, which indicates that the PEDOT:PSS modified by S-CNTs could also reduce the charge transport barrier and suppress the charge recombination, consequently resulting in the improvement of PCE. The hole mobilities of PEDOT:PSS:P-CNTs (0.2%) and PEDOT:PSS:S-Gra (0.2%) are 8.56×10^{-4} cm^2 V^{-1} s^{-1} and 4.93×10^{-4} cm^2 V^{-1} s^{-1}, respectively, which are lower than that of PEDOT:PSS:S-CNTs (0.2%) based on hole-only devices by SCLC method. Therefore, one-dimensional sulfonated carbon nanotubes as interface layer possesses an advantage over pristine CNTs and two-dimensional plane structure sulfonated graphenes. In addition, the PEDOT:PSS treated with sulfonated carbon materials at 2% weight ratio displays the best device performance.

The comparative ultraviolet photoelectron spectroscopy (UPS) spectra of the pristine and modified PEDOT:PSS and the energy level diagram of the device are shown in **Figure 2**. In contrast to the pristine PEDOT:PSS (-5.21 eV)[30], the work function of PEDOT:PSS:S-CNTs, PEDOT:PSS:DMSO, PEDOT:PSS:P-CNTs and PEDOT:PSS:S-Gra are -5.10 eV, -5.12 eV, -5.27 eV and -5.30 eV, respectively, without obvious change. It can be seen that the valence band energy levels of PEDOT:PSS:S-CNTs (-5.10 eV) is slightly higher than the HOMO energy level of P3HT donor (-5.20 eV), and low injection barrier between the PEDOT:PSS:S-CNTs and P3HT may be in favor of holes to be readily injected into PEDOT:PSS:S-CNTs

for collection by the ITO electrode. Moreover, PEDOT:PSS:P-CNTs and PEDOT:PSS:S-Gra show a little lower valence band energy levels than the HOMO energy level of donor, which may result in poor holes mobility and collection. The optical transmittance spectra of the pristine and modified PEDOT:PSS films on ITO glass at visible region (wavelength between 400 and 800 nm) are also shown in **Figure 2**. The pristine PEDOT:PSS and PEDOT:PSS:S-CNTs films present the same transmittance value (~90.5% at 550 nm), revealing that PEDOT:PSS film modified by S-CNTs as HTL could not affect the light absorption for the active layer. While P-CNTs and S-Gra added into PEDOT:PSS impair their transmittance, which leading to the lower short-circuit current density. The conductivities of the pristine and modified PEDOT:PSS films exhibiting a linear relationship with the applied voltage as shown in **Figure 2**, are compared from the slopes of the curve[31]. It can be seen that the conductivities of the modified PEDOT:PSS are enhanced by the incorporation sulfonated carbon materials, extremely for the PEDOT:PSS:S-Gra film. The reason may be that the stacked sulfonated graphenes with lamellar structure took the place of insulating excess PSS and provided bridges or networks among the insular and conductive PEDOT:PSS grains, which will be discussed detailedly in the later section. Although PEDOT:PSS:S-Gra shows highest conductivity compared to other modified PEDOT:PSS, it must be noted that the device performance based on PEDOT:PSS:S-Gra as HTL was inferior, compared with the PEDOT:PSS:S-CNTs. The stacked and crumpled lamellar graphenes in the PEDOT:PSS resulted in rough morphology which was unfavorable to form uniform active heterojunction.

To strengthen the aforementioned interpretation and gain further information for the improvement in device performance, the morphology of the pristine and modified

PEDOT:PSS was investigated by scan electron microscopy (SEM), as shown in **Figure S4**. Taking into consideration of the effect of DMSO solvent, the PEDOT:PSS:DMSO also was investigated to make a comparison, which makes unobvious changes on the morphology of PEDOT:PSS. The surface of the PEDOT:PSS:S-CNTs is uniform and smooth. However, the PEDOT:PSS modified by pristine CNTs has an irregular surface because of the agglomeration phenomenon. Meanwhile, PEDOT:PSS:S-Gra may form a severe unevenness morphology due to lamellar S-Gra stacks in PEDOT:PSS solution, which may result in an large current leakage (**Figure 1**). In order to complement the aforementioned morphological changes, the transmission electron microscopy (TEM) images of the pristine and modified PEDOT:PSS films were also investigated, as shown in **Figure 3**. DMSO was also added into PEDOT:PSS solution in order to exclude the solvent effect. In general, PEDOT:PSS grains consist of a PEDOT-rich core and PSS-rich shell. The pristine PEDOT:PSS has a smooth surface without phase separation and obvious agglomerated grains (or particles). DMSO and carbon materials modification enlarge the PEDOT grains. More importantly, in the PEDOT:PSS:S-CNTs, the shape of the dark PEDOT grains becomes a long stretched network in larger area with coincident to the subsequent atomic force microscopic (AFM) images in **Figure 4**, allowing the formation of more conductive PEDOT:PSS channels. Besides, the PEDOT:PSS:S-CNTs had an obvious phase separation with bigger PEDOT grains. However, in PEDOT:PSS:S-Gra, the big and stacked lamellar sulfonated graphenes can be found, without obvious phase separation and agglomerated PEDOT:PSS grains. Because of the strong π-π stacking interaction of graphenes inducing -SO_3H groups to uneffectively insert into the lamellar structure of graphenes, the resultant sulfonated graphenes (S-Gra) had only small amounts of -SO_3H groups attached to the edge of

graphenes. Weaker synergetic effcet between the S-Gra and PEDOT:PSS particles led to poor dispersibility of S-Gra in PEDOT:PSS solution, and consequently resulting in the rough morphology. In addition, the rough morphology of the interface layer also has an effect on the active morphology, and even induces changes to some extent. As shown in **Figure S5**, the surface morphology of P3HT:PCBM based on PEDOT:PSS:S-Gra becomes very rough. The root mean square (RMS) value increases to 3.98 nm from 2.80 nm in comparison to the active layer on top of the pristine PEDOT:PSS. The RMS of the active layer based on PEDOT:PSS:S-CNTs is 1.32 nm. The rougher active layer is unfavorable for the device performance. It renders insufficient phase separation of heterojunction for exciton disassociation. Therefore, it can be made clear that the inferior device performance based on PEDOT:PSS:S-Gra as HTL could be proved from the morphological analysis.

The role of PEDOT:PSS:S-CNTs as HTL in the enhancement of device performance and the interactions between S-CNTs and PEDOT:PSS are in-depth analyzed. **Figure 4** shows atomic force microscopy (AFM) topography and phase images of the pristine and modified PEDOT:PSS, respectively. In general, a spin-coated PEDOT:PSS solid film consists of PEDOT:PSS grains, with a hydrophobic and highly conductive PEDOT-rich core and a hydrophilic insulating PSS-rich shell[32]. The pristine PEDOT:PSS shows a typical morphology, in which the bright (positive) and dark (negative) phase shifts correspond to PEDOT-rich grains and PSS-rich grains[33,34], respectively, and the size of the disconnected conducting PEDOT-rich grains is small. For PEDOT:PSS:DMSO, PEDOT:PSS:P-CNTs and PEDOT:PSS:S-CNTs, the size and area of PEDOT-rich grains become bigger than that of pristine PEDOT:PSS. Moreover, bright PEDOT-rich grains in the PEDOT:PSS:S-CNTs transforms from the

isolated and small domains to a large stretched and continuous domains, while the dark PSS-rich regions become smaller with a distinct phase separation, indicating that the insulating PSS barrier surrounding is thinner. With comparison to PEDOT:PSS:P-CNTs, there are synergetic effect between -SO_3H groups of S-CNTs and PEDOT:PSS, weakening the interaction effect between the two components of PEDOT:PSS. The addition of S-CNTs into PEDOT:PSS can further give rise to the depletion of insulating PSS and formation of compact conductive PEDOT-rich granular networks, which generates larger contact areas among better oriented and continuous PEDOT-rich grains, consequently improving conducting pathways for carriers[35].

The interaction between S-CNTs and PEDOT:PSS would also improve hydrophobicity of the modified PEDOT:PSS, as shown in **Figure S6**. The optimized hydrophobicity of PEDOT:PSS:S-CNTs could result in better interface contact between the modified PEDOT:PSS and active layer, which would boost the device performance. The assumption of PSS depletion from the PEDOT:PSS film before and after film treatment with S-CNTs has been further supported by X-ray photoemission spectroscopy (XPS) and UV absorption spectra. **Figure 5** presents sulfur (S) 2p spectra and UV absorption spectra of the pristine and modified PEDOT:PSS films. The higher binding energy peaks at 169.0 eV and 167.8 eV and the lower binding energy peaks at 164.6 eV and 163.4 eV correspond to the sulfur atoms in PSS and PEDOT[32,36], respectively. By comparing the peak intensity of PSS and PEDOT for the pristine and modified PEDOT:PSS films, it can be calculated the ratios of PSS/PEDOT from the area ratios of $S2p_{1/2}$ and $S2p_{3/2}$ peaks in PSS and PEDOT, respectively, which are listed in **Table S1**. For the pristine PEDOT:PSS, the

PSS/PEDOT ratio is about 11.0. After the addition of P-CNTs and S-CNTs, the PSS/PEDOT molar ratios at the surface reduce in different degrees. For PEDOT:PSS:P-CNTs, the PSS/PEDOT ratio reduces to 8.6, nearly the same result as DMSO treatment. Because there is no obvious synergetic effect between PEDOT:PSS and pristine CNTs, so the depletion of PSS chains may be due to the DMSO solvent effect[37]. The PSS/PEDOT ratio of PEDOT:PSS:S-CNTs is about 7.5 and PSS content is markedly reduced by 31.8% calculated by XPS peaks. The reduction of PSS could be further confirmed by the UV absorption spectra in **Figure 5**. It can be seen that two absorption bands originated from the aromatic rings of PSS[38-40] drop off sharply after S-CNTs treatment, which effectively illustrating the depletion of hydrophilic and insulating PSS chains is attributed to the synergetic effect between S-CNTs and PEDOT:PSS. Because one-dimensional tubular S-CNTs with outstanding mechanical property, could break the PSS chains attached to the PEDOT and impair their interaction. Besides PEDOT molecules responsible for conduction in the blend are more uniformly distributed and continuous through the entire PEDOT:PSS film. Therefore, the depletion of insulating PSS chains leads to obvious phase separation between the PEDOT and PSS chains, which allowing the formation of more conductive PEDOT channels, and then improving the conductivity. In addition to the optimization of conductivity, the variations in PSS/PEDOT ratios at the surface of modified PEDOT:PSS films have played an important role in altering the interfacial layer morphology[33], which are in accordance with the aforementioned observations.

As mentioned previously, the increase of PEDOT ratio in the PEDOT:PSS:S-CNTs could also be observed in the Raman spectra, as shown in **Figure 6**. The strong 1442 cm^{-1} band of PEDOT is attributable to the ring C-C stretching vibration originating

from neutral parts exiting between localized elementary excitations such as positive polarons or bipolarons generated upon doping[41]. The peaks centered at 1508 cm^{-1} and 1570 cm^{-1} are assigned to the C=C asymmetric stretching vibrations in accordance with thiophene rings in the middle and at the end of the chains, respectively. The bands observed at 1255, 1367, 1505, 1539 and 1569 cm^{-1} are associated with PEDOT on the basis of the spectrum of PEDOT[42,43]. Upon the modification of S-CNTs, these bands increase clearly in intensity. Moreover, no bands of PSS are observed. Thus, the increase could be illustrated by the fact that the addition of S-CNTs in the PEDOT:PSS film could promote the PSS depletion, resulting in increasing the component of conductive PEDOT on film surface. From detailed analysis of these spectra, it has been observed that the peak position, peak width and intensity of the bands at 1539 and 1569 cm^{-1} in PEDOT:PSS:S-CNTs show an small shift and increase, compared with the pristine PEDOT:PSS, indicating the existence of interaction between S-CNTs and PEDOT:PSS.

Take into account the increase in conductivity of PEDOT:PSS solution treated with sulfonated carbon materials, the properties of the PEDOT:PSS (Clevious PH 1000) aqueous solution after the addition of S-CNTs and S-Gra were also investigated. The TEM and SEM images of the PH1000 films treated with 1% weight ratio are shown in **Figure S7**. The PH1000:DMSO film was also studied in order to exclude the effect of the solvent. The morphology of the modified PH1000:DMSO is smooth and uniform, and the wrinkled graphene lamellas can be found in the PH1000:S-Gra. Besides, the effects of incorporation S-CNTs and S-Gra on the sheet resistance and transmittance of the modified PH1000 films were also studied, as shown in **Figure 7**. It can be seen the sheet resistances of PH1000:S-CNTs and PH1000:S-Gra decrease greatly, which

are lower than the PH1000 and PH1000:DMSO. The PH1000:S-CNTs and PH1000:S-Gra possess sheet resistances of about 81.8 and 45 Ω sq^{-1} with the transmittance of 85.3% and 85.5% at 550 nm, respectively. In general, the transmittance of a transparent nanostructured metallic thin film is calculated using the following relationship:

$$T(\lambda) = (1 + \frac{188.5}{R_{sheet}} \frac{\sigma_{Op}(\lambda)}{\sigma_{DC}})^{-2} \quad \text{Eq (1)}$$

where σ_{Op} (λ) is the optical conductivity and σ_{DC} is the direct current (DC) conductivity of the film. Here, the ratio of σ_{DC}/σ_{Op} can be regarded as a figure of merit (FoM). The high values indicate the transparent conductive electrodes possesing desirable properties[44]. The PH1000:S-Gra film on a glass substrate exhibited σ_{DC}/σ_{Op} ≈51.6, which was greater than that for PH1000 film on a glass substrate (σ_{DC}/σ_{Op}≈ 16.3), as shown in **Table S2**. For PH1000:S-CNTs, the improvement in conductivity could also be attributed to the depletion of insulting PSS chains and conductive PEDOT aggregation due to the synergetic effect between S-CNTs and PEDOT:PSS. For PH1000:S-Gra, aside from the synergetic effect between S-Gra and PEDOT:PSS on the conductivity enhancement, the highly conductive sulfonated graphene lamellas may offer directly charge transport templates and build bridges or networks for connecting the insular and conductive PEDOT islands in the composites, resulting in a great improving in the conductivity of PH1000:S-Gra. And the UV absorption spectra (in **Figure S8**) of PH1000:S-CNTs and PH1000:S-Gra also demonstrated the depletion of PSS, with comparison to the pristine PH1000. These findings suggested that the different concentration PEDOT:PSS (Clevios PH 4083 and Clevios PH 1000) treated with sulfonated carbon materials both present prominent electrical properties and high transmittance. Moreover, the PH1000:S-Gra with high transmittance and low

sheet resistance due to the function of S-Gra as bridges for offering an continuous conducting pathways for electrons, is more suitable for applications as transparent conductive electrodes, which will be studied in detail later.

Conclusions

PEDOT:PSS modified by sulfonated carbon nanotubes (S-CNTs) and sulfonated graphenes (S-Gra) with sulfonic acid groups have been firstly investigated. The synergetic interaction of S-CNTs and S-Gra with PEDOT:PSS could remove excess insulating and hydrophilic PSS chains to generate obvious phase separation between the PEDOT and PSS chains, resulting in more conductive PEDOT channels, which in favor of enhancement in conductivity of PEDOT:PSS. Moreover, the conductive sulfonated graphene lamellas in the PEDOT:PSS:S-Gra composites may offer directly charge transport templates and build bridges or networks for connecting the insular and conductive PEDOT islands, and hence remarkably improve the conductivity further. The modified PEDOT:PSS:S-CNTs composites with well-matched work function, favorable morphology, optimized hydrophobicity, proper conductivity and higher hole mobility has been demonstrated to be an excellent hole transport layer (HTL) for polymer solar cells, showing the best photovoltaic performance with PCE values up to 3.91%, J_{sc} of 10.49 mA/cm^2, V_{oc} of 0.58 V, and FF of 64.1%. However, the device performance based on PEDOT:PSS:S-Gra as HTL was inferior, because the PEDOT:PSS modified with S-Gra formed a severe unevenness morphology attributed to the stacked and crumpled graphene lamellars in the PEDOT:PSS, which may impair current generation. Significantly, the modified PH1000:S-Gra composites with multiple layers can have sheet resistances of 45 Ω sq^{-1}and transparency over 85% at 550 nm, which may apply in organic electronics as conductive and flexible electrodes.

Acknowledgements

The financial supports for this work are provided by the National Natural Science Foundation of China (51273088 and 51302130) , National Basic Research Program of China (973 Program 2014CB260409), National Science Fund for Distinguished Young Scholars (51425304) and Doctoral Programs Foundation of Ministry of Education of China (Grants 20133601110004 and 20133601120006). Ting Ji and Licheng Tan contributed equally to this work.

Electronic supplementary information (ESI) available.

Experimental details such as the synthesis methods of sulfonated carbon nanotubes and sulfonated graphenes; The work function measurement of the pristine and modified PEDOT:PSS films; Space-charge-limited-current (SCLC) mobility measurement; The carbon materials characterization date; The SEM images of P-CNTs and S-CNTs in DMSO solvent; The SEM images and the contact angle of the pristine and modified PEDOT:PSS films; The AFM images of active layer based on PEDOT:PSS, PEDOT:PSS:S-CNTs, PEDOT:PSS:S-Gra; The SEM, TEM images and UV absorption spectra of the pristine and modified PH1000 films; Superficial PSS/PEDOT ratios of the pristine and modified PEDOT:PSS films.

References

(1) L. Chen, C. Xie, Y. Chen, *Macromolecules*, 2014, ***47***, 1623-1632.

(2) G. Yu, J. Gao, J. C. Hummelen, F. Wudl, AJ. Heeger, *Science*, 1995, ***270***, 1789-1790.

(3) J. You, L. Dou, K.Yoshimura, T. Kato, K. Ohya, T. Moriarty, K. Emery, C.-C. Chen, J.Gao, G. Li, Y. Yang, *Nat.Commun.*, 2013, ***4***, 1446.

(4) Y. Liu, C.-C. Chen, Z.Hong, J. Gao, Y. Yang, H. Zhou, L. Dou, G. Li, Y. Yang, *Sci. Rep.*, 2013, ***3***,3356-3356.

(5) M. Jørgensen, K. Norrman, S. A. Gevorgyan, T. Tromholt, B. Andreasen, F. C. Krebs, *Adv. Mater.*, 2012, ***24***, 580-612.

(6) M. Jørgensen, K. Norrman, F. C. Krebs, *Sol. Energy Mater. Sol. Cells*, 2008, ***92***, 686-714.

(7) L. Chen, C. Xie, Y. Chen, *Adv. Funct. Mater.*, 2014, ***24***, 3986-3995.

(8) E. Voroshazi, B. Verreet, A. Buri, R. Müller, D. Di Nuzzo, P. Heremans, *Org. Electron.*, 2011, ***12***, 736-744.

(9) F. C. Krebs, S. A. Gevorgyan, J. Alstrup, *J. Mater. Chem.*, 2009, ***19***, 5442-5451.

(10) J. Meyer, R. Khalandovsky, P. Görrn, A. Kahn, *Adv. Mater.*, 2011, ***23***, 70-73.

(11) H.-W. Lin, S.-W. Chiu, L.-Y. Lin, Z.-Y. Hung, Y.-H. Chen, F. Lin, K.-T. Wong, *Adv. Mater.*, 2012, ***24***, 2269-2272.

(12) S. Murase, Y. Yang, *Adv. Mater.*, 2012, ***24***, 2459-2462.

(13) F.-X. Xie, W. C. H. Choy, Wei E. I. Sha, D. Zhang, S. Zhang, X. Li, C.-w. Leung, J. Hou, *Energy Environ. Sci.*, 2013, ***6***, 3372-3379.

(14) G. Terán-Escobar, J. Pampel, J. M. Caicedo, M. Lira-Cantú, *Energy Environ. Sci.*, 2013, ***6***, 3088-3098.

(15) K. Lu, J. Yuan, J. Peng, X. Huang, L. Cui, Z. Jiang, H.-Q. Wang, W. Ma, *J. Mater. Chem.*, 2013, ***1***, 14253-14261.

(16) K. X. Steirer, P. F. Ndione, N. E. Widjonarko, M. T. Lloyd, J. Meyer, E. L. Ratcliff, A. Kahn, N. R. Armstrong, C. J. Curtis, D. S. Ginley, J. J. Berry, D. C. Olson, *Adv. Energy Mater.*, 2011, ***1***, 813-820.

(17) L. Zuo, X. Jiang, L. Yang, M. Xu, Y. Nan, Q. Yan, H. Chen, *Appl. Phys. Lett.*, 2011, ***99***, 183306-183306.

(18) T. Stubhan, N. Li, N. A. Luechinger, S. C. Halim, G. J. Matt, C. J. Brabec, *Adv. Energy Mater.*, 2012, ***2***, 1433-1438.

(19) N. Li, T. Stubhan, N. A. Luechinger, S. C. Halim, G. J. Matt, T. Ameri, C. J.

Brabec, *Org. Electron.*, 2012, ***13***, 2479-2484.

(20) H. Choi, B. Kim, M. J. Ko, D.-K. Lee, H. Kim, S. H. Kim, K. Kim, *Org. Electron.*, 2012, ***13***, 959-968.

(21) Y. Sun, C. J. Takacs, S. R. Cowan, J. H. Seo, X. Gong, A. Roy, A. J. Heeger, *Adv. Mater.*, 2011, ***23***, 2226-2230.

(22) N. A. D. Yamamoto, L. F. Lima, R. E. Perdomo, R. Valaski, V. L. Calil, A. G. Macedo, M. Cremona, L. S. Roman, *Chem. Phys. Lett.*, 2013, ***572***, 73-77.

(23) N. Kim, S. Kee, S. H. Lee, B. H. Lee, Y. H. Kahng, Y.-R. Jo, B.-J. Kim, K. Lee, *Adv. Mater.*, 2014, ***26***, 2268-2272.

(24) J. Zhang, L. Gao, J. Sun, Y. Liu, Y. Wang, J. Wang, Diam. Relat. Mater., 2012, ***22***, 82-87.

(25) D. J. Yun, S. W. Rhee, *ACS Appl. Mater. Interfaces*, 2012, ***4***, 982-989.

(26) D. J. Yun, K. Hong, S. Kim, W. M. Yun, J. Y. Jang, W. S. Kwon, C. E. Park, S. W. Rhee, *ACS Appl. Mater. Interfaces*, 2011, ***3***, 43-49.

(27) F. Liu, J. Sun, L. Zhu, X. Meng, C. Qi, F.-S. Xiao, *J. Mater. Chem.*, 2012, ***22***, 5495-5502.

(28) H. Yu, Y. Jin, Z. Li, F. Peng, H. Wang, *J. Solid State Chem.*, 2008, ***181***, 432-438.

(29) J. Liu, Y. Xue, L. Dai, *J. Phys. Chem. Lett.*, 2012, ***3***, 1928-1933.

(30) V. Shrotriya, G. Li, Y. Yao, C.-W. Chu, Y. Yang, *Appl. Phys. Lett.*, 2006, ***88***, 073508-073508.

(31) H. Pan, L. Zuo, W. Fu, C. Fan, B. Andreasen, X. Jiang, K. Norrman, F. C. Krebs, H. Chen, *Org. Electron.*, 2013, ***14***, 797-803.

(32) S.-I. Na, G. Wang, S.-S. Kim, T.-W. Kim, S.-H. Oh, B.-K. Yu, T. Lee, D.-Y. Kim, *J. Mater. Chem.*, 2009, ***19***, 9045-9053.

(33) A. M. Nardes, M. Kemerink, René A. J. Janssen, J. A. M. Bastiaansen, N. M. M. Kiggen, B. M. W. Langeved, A. J. J. M. van Breemen, M. M. de Kok, *Adv. Mater.*, 2007, ***19***, 1196-1200.

(34) M. Vosgueritchian, D. J. Lipomi, Z. Bao, *Adv. Energy Mater.*, 2012, ***22***, 421-428.

(35) Y. H. Kim, C. Sachse, M. L. Machala, C. May, L. Müller-Meskamp, K. Leo, *Adv. Funct. Mater.*, 2011, ***21***, 1076-1081.

(36) X. Crispin, F. L. E. Jakobsson, A. Crispin, P. C. M. Grim, P. Andersson, A. Volodin, C. van Haesendonck, M. van der Auweraer, W. R. Salaneck, M. Berggren, *Chem. Mater.*, 2006, ***18***, 4354-4360.

(37) N. K. Unsworth, I. Hancox, C. Argent Dearden, P. Sullivan, M. Walker, R. S.

Lilley, J. Sharp, T. S. Jones, *Org. Electron.*, 2014, ***15***, 2624-2631.

(38) D. Wakizaka, T. Fushimi, H. Ohkita, S. Ito, *Polymer*, 2004, ***10***, 8561-8565.

(39) Y. Xia, K. Sun, J. Ouyang, *Energy Environ. Sci.*, 2012, ***5***, 5325-5332.

(40) D. Alemu, H.-Y. Wei, K.-C. Ho, C.-W. Chu, *Energy Environ. Sci.*, 2012, ***5***, 9662-9671.

(41) M. Reyes-Reyes, I. Cruz-Cruz, R. López-Sandoval, *J. Phys. Chem. C.*, 2010, ***114***, 20220-20224.

(42) S. Sakamoto, M. Okumura, Z. Zhao, Y. Furukawa, *Chem. Phys. Lett.*, 2005, ***412***, 395-398.

(43) S. Garreau, G. Louarn, J. P. Buisson, G. Froyer, S. Lefrant, *Macromolecules*, 1999, ***32***, 6807-6812.

(44) M. Song, D. You, K. Lim, S. Park, S. Jung, C. S. Kim, D.-H. Kim, D.-G. Kim, J.-K Kim, J. Park, Y.-C. Kang, J. Heo, S.-H. Jin, J. H. Park, and J.-W Kang, *Adv. Funct. Mater.*, 2013, ***23***, 4177-4184.

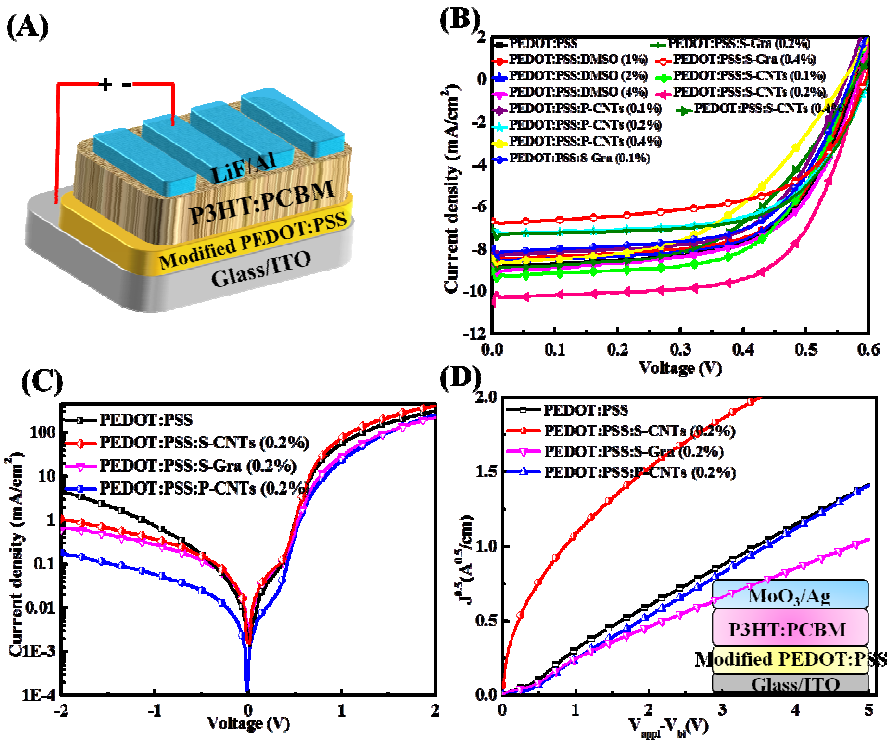

Figure 1. (A) The device structure, (B) current density-voltage (*J-V*) curves, (C) dark current of the devices based on pristine and modified PEDOT:PSS as HTL, and (D) $J^{0.5}$-V characteristics of hole-only devices with different PEDOT:PSS layers. The inset shows the hole-only devices structure. P-CNTs, S-CNTs and S-Gra were added into PEDOT:PSS at 0.1%, 0.2%, 0.4% weight ratio. To make a comparison, PEDOT:PSS was treated by DMSO solvent with the same volume ratio (1%, 2%, 4%) as the carbon materials dispersion.

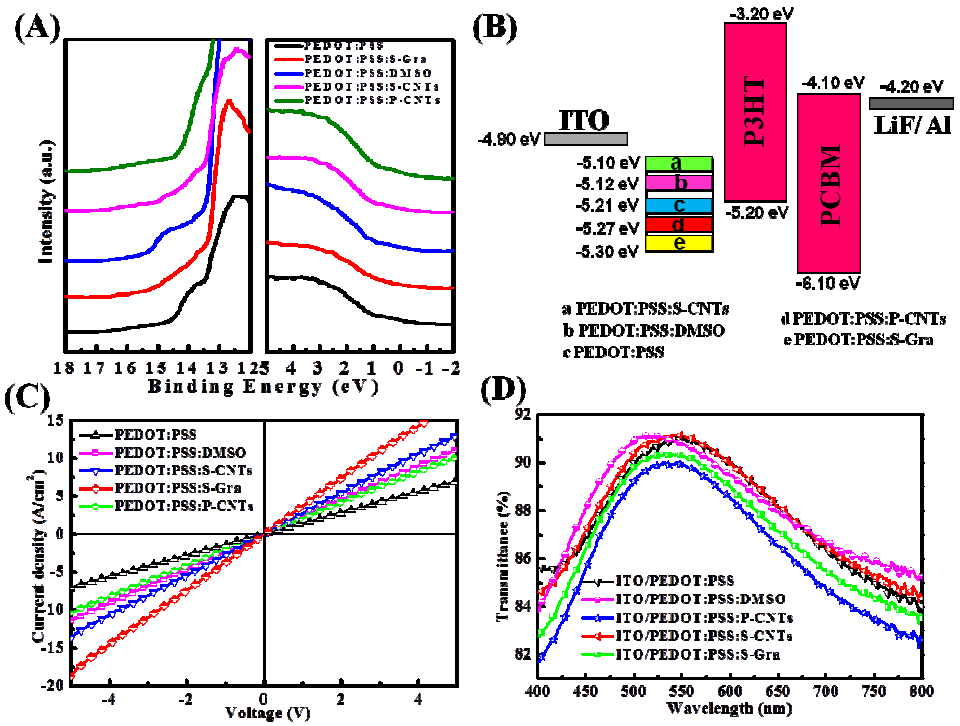

Figure 2. (A) Work function of the pristine and modified PEDOT:PSS coated ITO measured by UPS, (B) energy level diagram of the device, (C) conductivity and (D) transmittance of the pristine and modified PEDOT:PSS. The electric conductivity device configuration: ITO/pristine and modified PEDOT:PSS/Ag. P-CNTs, S-CNTs and S-Gra were added into PEDOT:PSS at 0.2% weight ratio. To make a comparison, PEDOT:PSS was treated by DMSO with the same volume ratio (2%) as carbon materials dispersion.

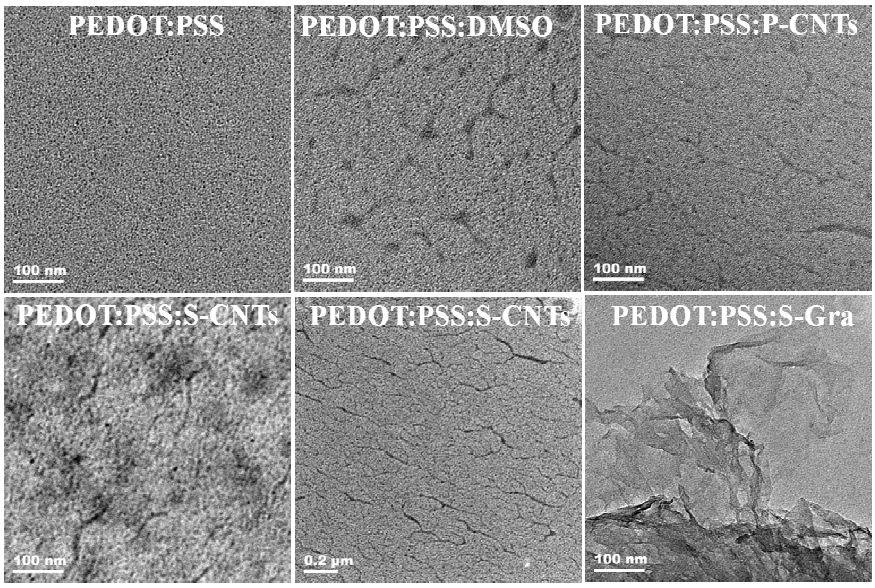

Figure 3. TEM images of the pristine and modified PEDOT:PSS. P-CNTs, S-CNTs and S-Gra were added into PEDOT:PSS at 0.2% weight ratio. To make a comparison, PEDOT:PSS was treated with DMSO at same ratio.

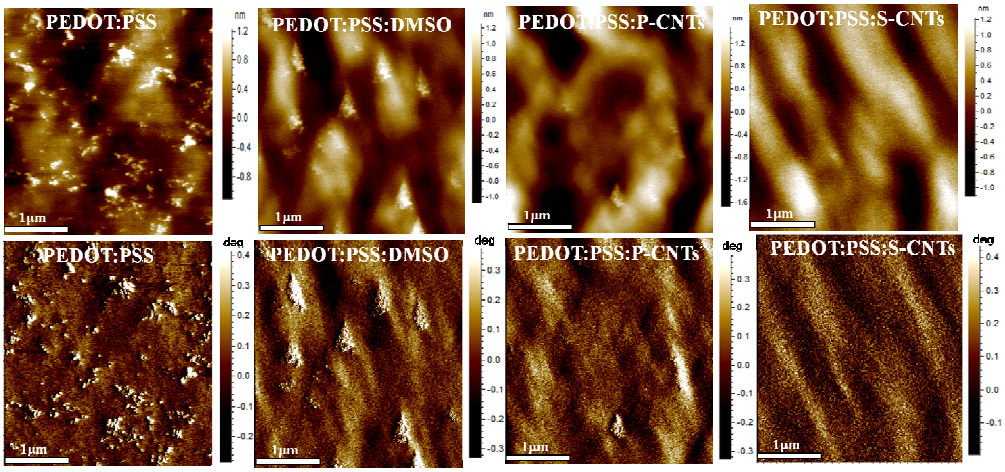

Figure 4. AFM (topography and phase) images of the pristine and modified PEDOT:PSS. P-CNTs, S-CNTs and S-Gra were added into PEDOT:PSS at 0.2% weight ratio. To make a comparison, PEDOT:PSS was treated with DMSO at same ratio.

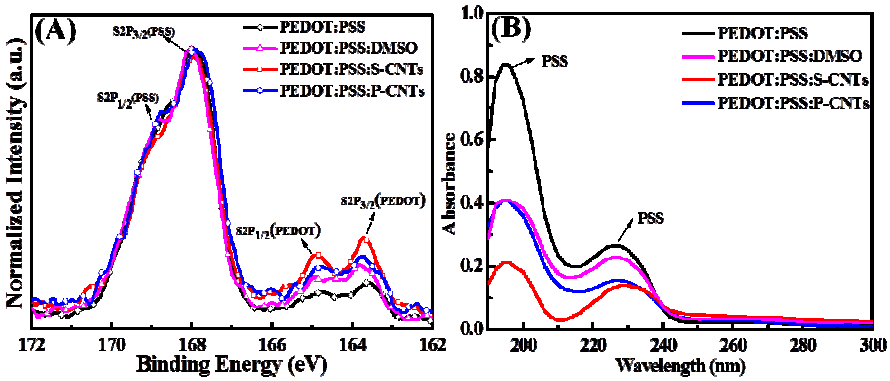

Figure 5. (A) XPS (S2p) and (B) UV absorption spectra of the pristine and modified PEDOT:PSS. P-CNTs, S-CNTs and S-Gra were added into PEDOT:PSS at 0.2% weight ratio. To make a comparison, PEDOT:PSS was treated with DMSO at same ratio.

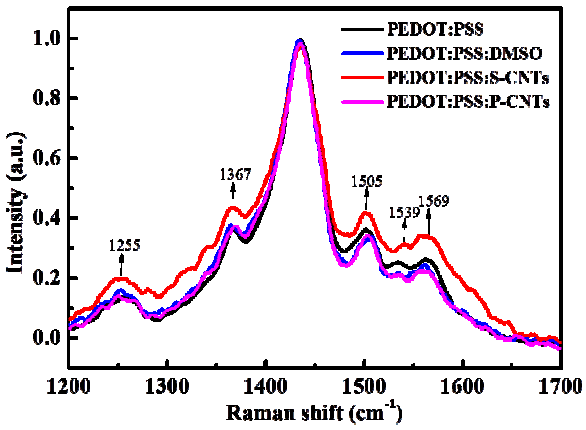

Figure 6. Raman spectra of the pristine and modified PEDOT:PSS. P-CNTs, S-CNTs and S-Gra were added into PEDOT:PSS at 0.2% weight ratio. To make a comparison, PEDOT:PSS was treated with DMSO at same ratio.

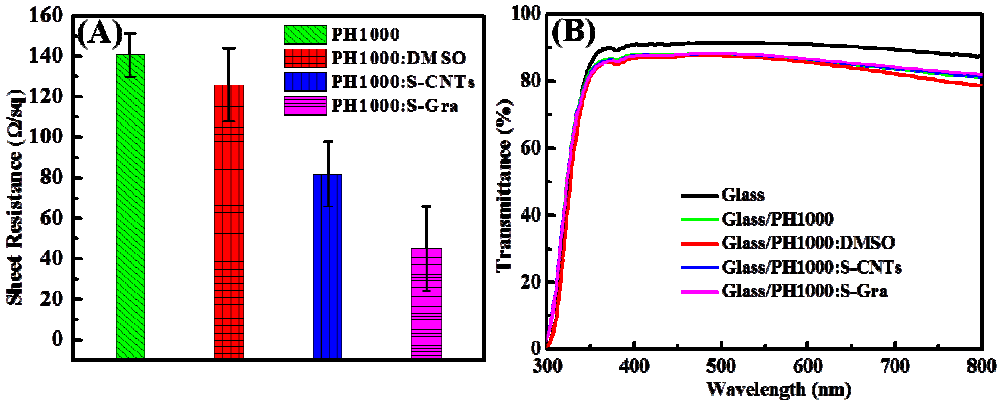

Figure 7. (A) The sheet resistance and (B) transmittance in the visible region (300-800 wavelength) of the pristine and modified PH1000. S-CNTs and S-Gra were added into PEDOT:PSS at 1.0% weight ratio. To make a comparison, PEDOT:PSS was treated with DMSO at same ratio.

Table 1. Device performance of P3HT:PCBM solar cells fabricated with different hole transport layers under AM 1.5 illumination of 100 mW/cm^{2}[a].

Hole transport layers	V_{oc} (V)	J_{sc} (mA/cm^{2})	FF (%)	PCE (%)
PEDOT:PSS	0.58±0.02	8.95±0.12	60.7±0.32	3.15±0.09 (3.20)[b]
PEDOT:PSS:DMSO (1%)	0.57±0.02	8.54±0.15	63.0±0.36	3.10±0.11 (3.15)[b]
PEDOT:PSS:DMSO (2%)	0.57±0.03	8.87±0.13	60.5±0.12	3.10±0.12 (3.14)[b]
PEDOT:PSS:DMSO (4%)	0.58±0.03	8.77±0.02	62.1±0.20	3.15±0.10 (3.16)[b]
PEDOT:PSS:S-CNTs (0.1%)	0.57±0.02	9.05±0.04	62.9±0.21	3.24±0.10 (3.28)[b]
PEDOT:PSS:S-CNTs (0.2%)	0.58±0.03	10.49±0.05	64.1±0.35	3.91±0.03 (3.96)[b]
PEDOT:PSS:S-CNTs (0.4%)	0.58±0.02	8.51±0.06	55.4±1.10	2.75±0.08 (2.80)[b]
PEDOT:PSS:P-CNTs (0.1%)	0.56±0.02	8.36±0.11	60.5±0.26	2.83±0.12 (2.85)[b]
PEDOT:PSS:P-CNTs (0.2%)	0.59±0.02	7.15±0.14	62.4±0.30	2.63±0.11 (2.70)[b]
PEDOT:PSS:P-CNTs (0.4%)	0.56±0.03	8.45±0.12	50.8±0.28	2.42±0.08 (2.51)[b]
PEDOT:PSS:S-Gra (0.1%)	0.59±0.02	7.52±0.13	61.0±0.19	2.70±0.13 (2.76)[b]
PEDOT:PSS:S-Gra (0.2%)	0.57±0.03	7.95±0.12	62.9±0.15	2.90±0.11 (2.96)[b]
PEDOT:PSS:S-Gra (0.4%)	0.59±0.02	6.67±0.14	60.0±0.28	2.40±0.12 (2.50)[b]

[a]All values represent averages from twelve 4 mm^{2} devices on a single chip, and the areas were tested with an aperture. [b]Best device PCE.

Highlights

A Comprehensive Study of Sulfonated Carbon Materials as Conductive Composites for Polymer Solar Cells

Ting Ji, Licheng Tan, Xiaotian Hu, Yanfeng Dai, Yiwang Chen*

The sulfonated graphenes lamellars are favorable to bridge the PEDOT islands, hence significantly improve the conductivity.

Graphical abstract